RECEIVER DESIGN FOR DOPPLER POSITIONING WITH LEO SATELLITES

Joe J. Khalife
Department of Electrical Engineering and Computer Science
University of California, Irvine, CA, USA
khalifej@uci.edu

*Zaher M. Kassas**
Department of Mechanical and Aerospace Engineering
University of California, Irvine, CA, USA
zkassas@ieee.org

ABSTRACT

A framework for positioning with low Earth orbit (LEO) satellite signals is proposed. The framework employs an extend Kalman filter (EKF) to estimate a receiver's position using Doppler frequency measurements from LEO satellites. The satellites' positions and velocities are known through two-line element (TLE) files. A receiver architecture to acquire and track LEO satellite signals and extract Doppler measurements to LEO satellites is discussed. Simulation results show that 11 m positioning accuracy can be achieved with 25 LEO satellites. Experimental results are presented demonstrating the proposed stationary receiver estimating its position using Doppler measurements from 2 Orbcomm LEO satellites with an accuracy of 360 m over a 1 minute period.

***Index Terms*—** Doppler positioning, quadrature phase shift keying modulation, low Earth orbit satellite communication.

1. INTRODUCTION

Global navigation satellite systems (GNSS) has been at the heart of outdoor positioning systems. However, GNSS signals could become unusable (e.g., indoors [1], in deep urban canyons, near dense foliage, and in the presence of unintentional interference or intentional jamming [2]) or untrustworthy (e.g., during malicious spoofing attacks [3]). The potential of using signals of opportunity (SOPs) as alternative navigation sources during GNSS unavailability has been the subject of extensive research recently [4, 5]. Example SOPs include AM/FM radio [6, 7], low Earth orbit (LEO) satellites [8–12], WiFi [13, 14], and cellular [15–19].

LEO satellites possess desirable attributes for positioning in GNSS-challenged environments: 1) they are around twenty times closer to the Earth compared to GNSS satellites, which reside in medium Earth orbit (MEO), making their received signal power between 24 to 34 dBs higher than GNSS signals; 2) they will become abundant as OneWeb, SpaceX, Boeing, and others plan to aggregately launch thousands of broadband Internet satellites into LEO [20]; and 3) each of these broadband providers will deploy broadband Internet satellites into unique constellations, transmitting at different frequency bands, making LEO satellite signals diverse in frequency and direction [21]. Moreover, the Keplerian elements parameterizing the orbits of these LEO satellites are made publicly available by the North American Aerospace Defense Command (NORAD) and are updated daily in the two-line element (TLE) files. Using TLEs and orbit determination algorithms (e.g., SGP 4), the positions and velocities of these satellites can be known, albeit not precisely.

*Professor Kassas is also with the Department of Electrical Engineering and Computer Science at the University of California, Irvine, CA, USA. This work was supported in part by the Office of Naval Research (ONR) under Grant N00014-16-1-2305.

LEO satellite SOPs are not intended for navigation. As such, three main challenges must be addressed to use their signals for navigation: 1) design specialized receivers that can extract navigation observables from these signals, 2) develop navigation frameworks that can account for the unknown nature of the LEO satellite SOP states (namely clock bias, drift, and/or position and velocity), and 3) characterize their error budgets. This paper tackles the first two challenges for LEO satellites transmitting direct quadrature phase shift-keying (QPSK) signals by discussing a receiver architecture to extract Doppler measurements from such signals and proposing a framework for positioning with the LEO satellite Doppler measurements. It is important to note that Doppler positioning has been considered since the conception of satellite-based navigation, e.g., the TRANSIT system. However, such systems were designed for navigation and did not pose any of the aforementioned challenges since TRANSIT satellites 1) transmit unmodulated tones and 2) provide clock bias and drift corrections and precise orbital elements to the receiver.

Extracting Doppler measurements from QPSK signals transmitted by LEO satellites can be achieved through carrier synchronization, a topic well discussed in the signal processing literature [22, 23]. However, since these signals are being used opportunistically, one cannot assume that the receiver and satellites' clocks are synchronized. Therefore, the receiver's and satellite transmitters' clock drifts must be accounted for. The methods proposed in the literature on Doppler positioning with LEO satellites either assume no clock drifts or assume round-trip-type measurements [24, 25]. In contrast to these assumptions, this paper proposes a Doppler positioning framework with LEO satellites that accounts for the drifts in the receiver's and LEO satellites' clocks. An extended Kalman filter (EKF) is employed to simultaneously estimate the receiver's position and the difference between the receiver's and each of the LEO satellites' clock drifts. Simulation and experimental results are presented demonstrating the proposed framework.

The paper is organized as follows. Section 2 formulates the positioning problem, describes the pseudorange rate and altimeter measurement models, and formulates the EKF. Section 3 discusses a receiver architecture to acquire and track LEO satellite signals and extract pseudorange rates to LEO satellites. Section 4 presents simulation and experimental results demonstrating the proposed framework. Concluding remarks are given in Section 5.

2. MODEL DESCRIPTION

2.1. Problem Formulation

This paper considers a stationary radio frequency (RF) receiver equipped with an altimeter. The receiver listens to multiple LEO satellite downlink channels, where direct QPSK signals are transmitted. The receiver makes Doppler frequency measurements to

each of the available LEO satellites and uses these measurements along with alitmeter measurements to estimate its position using an EKF. The models employed in the paper are described next, namely models for: the receiver's position and clock drift dynamics, the LEO satellites' clock drifts dynamics, and the pseudorange rate and altimeter measurements. The EKF is then formulated.

2.2. Receiver and LEO Satellite Clock Dynamics

The receiver state consists of its three-dimensional (3–D) position vector $\boldsymbol{r}_r \triangleq [x_r, y_r, z_r]^{\mathsf{T}}$ and its clock drift $\dot{\delta}t_r$. The receiver is assumed to be stationary with a constant clock drift. It is also assumed that the LEO satellites' clock drifts $\left\{\dot{\delta}t_{\mathrm{leo},l}\right\}_{l=1}^{L}$ are constant, where L is the total number of available LEO satellites. The 3–D position and velocity vectors of the l-th LEO satellite at time-step k are given by $\boldsymbol{r}_{\mathrm{leo},l}(k)$ and $\dot{\boldsymbol{r}}_{\mathrm{leo},l}(k)$, respectively, which are obtained using TLE files and SGP 4 orbit determination software.

2.3. Pseudorange Rate Measurement Model

The receiver produces pseudorange rate measurements to the l-th satellite, which can be related to the Doppler frequency at time-step k using

$$z_{\mathrm{leo},l}(k) \triangleq c\frac{\hat{f}_{D_l}(k)}{f_{c,l}}, \quad l = 1, \ldots, L, \quad k = 0, 1, \ldots, \qquad (1)$$

where $\hat{f}_{D_l}$ is the measured Doppler frequency to the l-th satellite, $f_{c,l}$ is the carrier frequency at which the l-th satellite is transmitting, and c is the speed of light. The pseudorange rate measurement to the l-th satellite can be expressed as

$$\begin{aligned} z_{\mathrm{leo},l}(k) =& \frac{\dot{\boldsymbol{r}}_{\mathrm{leo},l}^{\mathsf{T}}(k)\left[\boldsymbol{r}_r - \boldsymbol{r}_{\mathrm{leo},l}(k)\right]}{\|\boldsymbol{r}_r - \boldsymbol{r}_{\mathrm{leo},l}(k)\|} + c\Delta\dot{\delta}t_l \\ &+ c\left[\dot{\delta}t_{\mathrm{iono},l}(k) + \dot{\delta}t_{\mathrm{trop},l}(k)\right] + v_{\mathrm{leo},l}(k), \end{aligned}$$

where $\Delta\dot{\delta}t_l \triangleq \dot{\delta}t_r - \dot{\delta}t_{\mathrm{leo},l}$, $\dot{\delta}t_{\mathrm{iono},l}$ and $\dot{\delta}t_{\mathrm{trop},l}$ are the l-th satellite's ionospheric and tropospheric delay rates, respectively, and $v_{\mathrm{leo},l}$ is the measurement noise, which is modeled as a zero-mean white Gaussian random sequence with variance $\sigma^2_{\mathrm{leo},l}$. Note that the variations in the ionospheric and tropospheric delays during LEO satellite visibility are negligible compared to the errors in the satellite's estimated velocities; hence, $\dot{\delta}t_{\mathrm{iono}_l}$ and $\dot{\delta}t_{\mathrm{trop}_l}$ are ignored in the measurement, yielding the measurement model given by

$$z_{\mathrm{leo},l}(k) \approx \frac{\dot{\boldsymbol{r}}_{\mathrm{leo},l}^{\mathsf{T}}(k)\left[\boldsymbol{r}_r - \boldsymbol{r}_{\mathrm{leo},l}(k)\right]}{\|\boldsymbol{r}_r - \boldsymbol{r}_{\mathrm{leo},l}(k)\|} + c\Delta\dot{\delta}t_l + v_{\mathrm{leo},l}(k). \qquad (2)$$

The vector of all available pseudorange rate measurements at time-step k is defined as $\boldsymbol{z}_{\mathrm{leo}}(k) \triangleq [z_{\mathrm{leo},1}(k), \ldots, z_{\mathrm{leo},L}(k)]^{\mathsf{T}}$.

2.4. Receiver Altimeter Measurement Model

The receiver is assumed to be equipped with an altimeter which produces the measurements given by

$$z_{\mathrm{alt}}(k) = z_r + v_{\mathrm{alt}}(k), \qquad (3)$$

where v_{alt} is the measurement noise, which is modeled as a zero-mean white Gaussian random sequence with variance σ^2_{alt}.

2.5. EKF Model

From (2), it can be seen that the state to be estimated is $\boldsymbol{x} \triangleq \left[\boldsymbol{r}_r^{\mathsf{T}}, c\Delta\dot{\delta}t_1, \ldots, c\Delta\dot{\delta}t_L\right]^{\mathsf{T}}$. Subsequently, an EKF is designed to produce an estimate $\hat{\boldsymbol{x}}(k|m)$ of $\boldsymbol{x}(k)$ using all pseudorange rate and altimeter measurements from time-step 1 to $m \leq k$, i.e, $\mathbf{Z}^m \triangleq \{\boldsymbol{z}(m')\}_{m'=1}^{m}$, where $\boldsymbol{z}(m') \triangleq \left[\boldsymbol{z}_{\mathrm{leo}}^{\mathsf{T}}(m'), z_{\mathrm{alt}}(m')\right]^{\mathsf{T}}$. The estimation error is denoted $\tilde{\boldsymbol{x}}(k|m) \triangleq \boldsymbol{x}(k) - \hat{\boldsymbol{x}}(k|m)$. The EKF also calculates the estimation error covariance $\mathbf{P}(k|m) \triangleq \mathbb{E}\left[\tilde{\boldsymbol{x}}(k|m)\tilde{\boldsymbol{x}}^{\mathsf{T}}(k|m)\right]$. Given a prior $\hat{\boldsymbol{x}}(0|0)$ and $\mathbf{P}(0|0)$, the standard EKF equations are iterated. The EKF state and estimation error covariance time-update equations are given by

$$\hat{\boldsymbol{x}}(k+1|k) = \hat{\boldsymbol{x}}(k|k), \quad \mathbf{P}(k+1|k) = \mathbf{P}(k|k) + \mathbf{Q},$$

where $\mathbf{Q}$ is the process noise covariance. Note that since $\boldsymbol{x}$ is a constant vector, $\mathbf{Q}$ is theoretically a zero matrix. However, in order to prevent the estimation error covariance from converging to zero, $\mathbf{Q}$ is chosen to be $\mathbf{Q} \equiv \epsilon\mathbf{I}_{(3+L)\times(3+L)}$ where ϵ is a very small positive number. Given an innovation vector $\boldsymbol{\nu}(k+1)$, the state and covariance measurement update equations are given by

$$\begin{aligned} \hat{\boldsymbol{x}}(k+1|k+1) &= \hat{\boldsymbol{x}}(k+1|k) + \mathbf{K}(k+1)\boldsymbol{\nu}(k+1), \\ \mathbf{P}(k+1|k+1) &= \left[\mathbf{I} - \mathbf{K}(k+1)\mathbf{H}(k+1)\right]\mathbf{P}(k+1|k), \end{aligned}$$

where $\mathbf{K}(k+1)$ is the standard Kalman gain, $\mathbf{H}(k+1)$ is the measurement Jacobian given by

$$\mathbf{H}(k+1) = \left[\boldsymbol{h}_{\mathrm{leo},1}(k+1) \quad \ldots \quad \boldsymbol{h}_{\mathrm{leo},L}(k+1) \quad \boldsymbol{h}_{\mathrm{alt}}\right]^{\mathsf{T}},$$

$$\boldsymbol{h}_{\mathrm{leo},l}(k+1) \triangleq \left[\boldsymbol{h}_{r,l}^{\mathsf{T}}(k+1), \boldsymbol{e}_l^{\mathsf{T}}\right]^{\mathsf{T}}, \quad \boldsymbol{h}_{\mathrm{alt}} \triangleq [0, 0, 1, \mathbf{0}_{1\times L}]^{\mathsf{T}},$$

where $\boldsymbol{e}_l$ is an $L\times 1$ vector whose l-th element is 1 and the rest 0,

$$\begin{aligned} \boldsymbol{h}_{r,l}(k) \triangleq& \frac{\dot{\boldsymbol{r}}_{\mathrm{leo},l}(k+1)}{\|\hat{\boldsymbol{r}}_r(k+1|k) - \boldsymbol{r}_{\mathrm{leo},l}(k+1)\|} \\ &- \left[\hat{\boldsymbol{r}}_r(k+1|k) - \boldsymbol{r}_{\mathrm{leo},l}(k+1)\right] \\ &\times \frac{\dot{\boldsymbol{r}}_{\mathrm{leo},l}^{\mathsf{T}}(k+1)\left[\hat{\boldsymbol{r}}_r(k+1|k) - \boldsymbol{r}_{\mathrm{leo},l}(k+1)\right]}{\|\hat{\boldsymbol{r}}_r(k+1|k) - \boldsymbol{r}_{\mathrm{leo},l}(k+1)\|^3}, \end{aligned}$$

and $\hat{\boldsymbol{r}}_r(k+1|k)$ is the receiver's position prediction at time-step $k+1$. The innovation vector $\boldsymbol{\nu}(k+1)$ is formed according to

$$\boldsymbol{\nu}(k+1) = \left[\nu_{\mathrm{leo},1}(k+1), \ldots, \nu_{\mathrm{leo},L}(k+1), \nu_{\mathrm{alt}}(k+1)\right]^{\mathsf{T}},$$

where $\nu_{\mathrm{alt}}(k+1) = z_{\mathrm{alt}}(k+1) - \hat{z}_r(k+1|k)$ and $\nu_{\mathrm{leo},l}(k+1) = z_{\mathrm{leo},l}(k+1) - \hat{z}_{\mathrm{leo},l}(k+1)$, where

$$\begin{aligned} \hat{z}_{\mathrm{leo},l}(k+1) =& \frac{\dot{\boldsymbol{r}}_{\mathrm{leo},l}^{\mathsf{T}}(k+1)\left[\hat{\boldsymbol{r}}_r(k+1|k) - \boldsymbol{r}_{\mathrm{leo},l}(k+1)\right]}{\|\hat{\boldsymbol{r}}_r(k+1|k) - \boldsymbol{r}_{\mathrm{leo},l}(k+1)\|} \\ &+ c\Delta\hat{\dot{\delta}}t_l(k+1|k). \end{aligned}$$

Remark The same framework may be employed for a mobile receiver with known dynamics by accordingly modifying the EKF state vector, time-update equations, and the measurement Jacobian.

3. LEO SATELLITE NAVIGATION RECEIVER DESIGN

This section describes a receiver architecture for navigation with LEO satellites transmitting direct QPSK signals. Throughout this section, it is assumed that the LEO satellite signals are propagating in an additive white complex Gaussian channel with total power spectral density N_0.

3.1. Signal Model

The receiver simultaneously samples the bandwidth containing all LEO satellite downlink channels with a sampling period T. The received signal may be modeled as

$$r(i) = \sum_{l=1}^{L} s_l(i) + n(i), \quad i = 0, 1, \ldots,$$

where $n(i) \triangleq n_I(i) + jn_Q(i)$, n_I and n_Q are modeled as zero-mean white Gaussian noise with variance $\frac{N_0}{2T}$, and

$$s_l(i) \triangleq \sqrt{C_l} a_l(i) \exp\left\{j2\pi \left[f_{D,l}(i) + f_{\mathrm{IF},l}\right] iT + j\theta_l(i)\right\},$$

where C_l is the received signal power on the l-th channel, $a_l \triangleq \exp\left[j\left(\frac{u\pi}{2} + \frac{\pi}{4}\right)\right]$ for $u \in \{0, 1, 2, 3\}$ is the transmitted QPSK symbol on the l-th channel, $f_{D,l}$ is the Doppler shift in the l-th channel, $f_{\mathrm{IF},l}$ is the l-th channel intermediate frequency, and θ_l is the l-th channel carrier phase shift. The time argument i implies that the corresponding quantity is evaluated at time $t_i \triangleq t_0 + iT$ for some initial time t_0. The QPSK symbol period is T_{symb}, which is related to the sampling period through $T_{\mathrm{symb}} = MT$, where M is a large integer. It is assumed that the Doppler and carrier phase shifts are constant over T_{symb}. The signal in the l-th channel may be retrieved by mixing $r(i)$ with the corresponding intermediate frequency and passing the resulting signal through a low-pass filter (LPF) with bandwidth $B_l > \frac{2}{T_{\mathrm{symb}}}$, yielding

$$r_l(i) = \sqrt{C_l} a_l(k) \exp[j2\pi f_{D,l}(k) iT + j\theta_l(k)] + n_l(i), \; i = 0, 1, \ldots,$$

where $k \triangleq \left\lfloor \frac{i}{M} \right\rfloor$, $n_l(i) \triangleq n_{I,l}(i) + jn_{Q,l}(i)$, and $n_{I,l}$ and $n_{Q,l}$ are zero-mean white Gaussian noise with variance $\frac{N_0 B_l}{2}$. The time argument k implies that the corresponding quantity is evaluated at time $t_k \triangleq t_0 + kT_{\mathrm{symb}}$. The LPFs' bandwidths $\{B_l\}_{l=1}^{L}$ are chosen to be large enough to account for the Doppler shift. For Orbcomm LEO satellites, this shift can be between -3 kHz and 3 kHz.

3.2. Navigation Receiver Architecture

The navigation receiver employs independent phase-locked loops (PLLs) to track the LEO satellite signal on each of the L channels. The Doppler shifts produced by the PLLs are then passed to the navigation filter, which can be an EKF or a weighted nonlinear least-squares (WNLS) estimator, as shown in Fig. 1(a). Each tracking loop is a feedback loop that consists of an integrate and dump (I&D) filter, a phase discriminator, a loop filter, and a numerically controlled oscillator (NCO), as shown in Fig. 1(b).

Denote $\hat{\theta}_l(k)$ the current phase estimate maintained by the l-th channel's NCO and $\hat{f}_{D,l}(k)$ the current Doppler shift estimate maintained by the PLL. Then, between time-steps k and $k+1$, M samples of $r_l(i)$ are mixed with the estimated residual carrier wave due to Doppler and coherently summed over T_{symb} yielding

$$\begin{aligned}\hat{s}_l(k+1) &= \frac{1}{M} \sum_{i=i_0}^{i_0+M-1} r_l(i) \exp\left[j2\pi \hat{f}_{D,l}(k) iT + j\hat{\theta}_l(k)\right] \\ &\approx \sqrt{C_l} a_l(k+1) \exp\left[j\Delta\theta_l(k+1)\right] + \hat{n}_l(k),\end{aligned}$$

where $\Delta\theta_l(k+1)$ is the phase error at time-step $k+1$, $\hat{n}_l(k) \triangleq \hat{n}_{I,l}(k) + j\hat{n}_{Q,l}(k)$, and $\hat{n}_{I,l}$ and $\hat{n}_{Q,l}$ are zero-mean white Gaussian noise with variance $\frac{N_0}{2T_{\mathrm{symb}}}$. Note that $\hat{\theta}_l$ is updated according to

$$\hat{\theta}_l(k+1) = \hat{\theta}_l(k) + 2\pi \hat{f}_{D,l}(k) MT, \qquad \hat{\theta}_l(0) \equiv 0.$$

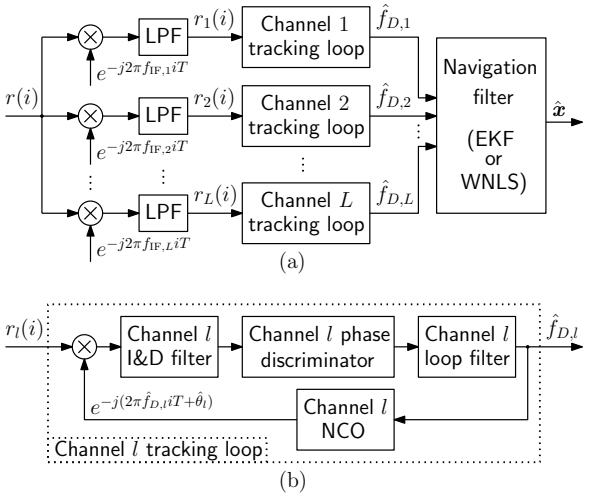

Fig. 1. Navigation receiver: (a) Each channel is first extracted then fed to a tracking loop. The resulting Doppler measurements are passed to the navigation filter. (b) Tracking loop for the l-th channel.

Given $\hat{s}_l(k+1)$, $\Delta\theta_l(k+1)$ can be obtained using a QPSK phase discriminator. A maximum-likelihood discriminator is employed in this paper, given by

$$\Delta\theta_l(k) = \frac{1}{\sqrt{C_l}} \left\{Q_l(k) \tanh\left[I_l(k)\right] - I_l(k) \tanh\left[Q_l(k)\right]\right\},$$

where $I_l(k)$ and $Q_l(k)$ are the real and imaginary parts of $\hat{s}_l(k)$, respectively, and $\tanh$ is the hyperbolic tangent function [26].

The phase error at time-step $k+1$ is then passed through the loop filter, which is a first-order filter with the continuous-time transfer function $F(s) = \frac{2\zeta\omega_n s + \omega_n^2}{s}$, where $\zeta \equiv \frac{1}{\sqrt{2}}$ is the damping ratio and ω_n is the undamped natural frequency, which can be related to the PLL noise-equivalent bandwidth $B_{n,\mathrm{PLL}}$ by $B_{n,\mathrm{PLL}} = \frac{\omega_n}{8\zeta}\left(4\zeta^2 + 1\right)$. Denote $v_{\mathrm{PLL},l}$ the output of the filter. The Doppler frequency estimate $\hat{f}_{D,l}(k+1)$ is deduced by dividing $v_{\mathrm{PLL},l}(k+1)$ by 2π. The loop filter transfer function is discretized and realized in state-space. The measurement vector $\boldsymbol{z}_{\mathrm{leo}}$ is formed using the Doppler shift estimates tracked by each PLL according to (1) to perform the EKF measurement update.

It can be shown that the noise variance $\sigma^2_{\Delta\theta,l}$ of the maximum-likelihood discriminator can be expressed as [26]

$$\sigma^2_{\Delta\theta,l} = \frac{1}{\mathrm{SNR}_l^3}\left(\frac{8}{9\mathrm{SNR}_l^4} + \frac{20}{3\mathrm{SNR}_l^3} + \frac{10}{3\mathrm{SNR}_l^2} - \frac{8}{3\mathrm{SNR}_l} + 2\right), \quad (4)$$

where $\mathrm{SNR}_l = \frac{C_l T_{\mathrm{symb}}}{N_0}$ is the signal-to-noise ratio (SNR) on the l-th channel. It can be shown that the variance of the closed-loop PLL noise is given by $\sigma^2_{\mathrm{PLL},l} = 2\sigma^2_{\Delta\theta,l} B_{n,\mathrm{PLL}} T_{\mathrm{symb}}$, from which the pseudorange rate measurement noise variance can be found to be

$$\sigma^2_{\mathrm{leo},l} = \frac{2c^2}{f^2_{c,l}} \sigma^2_{\Delta\theta,l} B_{n,\mathrm{PLL}} T_{\mathrm{symb}}. \quad (5)$$

3.3. Signal Acquisition

An initial Doppler estimate is needed to initialize the tracking loops. To this end, the Fast Fourier Transform (FFT) method is used to acquire the Doppler frequency for each channel [27].

ΔT \ L	5	10	15	20	25
1 minute	168.53	100.78	74.01	55.52	37.95
2 minutes	111.25	84.12	50.03	31.34	20.27
4 minutes	28.30	27.10	20.93	17.63	11.38

Table 1. RMSEs (in meters) from 100 Monte Carlo runs for varying number of available LEO satellites L and positioning duration ΔT.

Denote $R_{\eta,l}(K)$ the FFT of $r_l(i)$ for $i = \eta M + i_0, \ldots, (\eta + 1)M + i_0 - 1$ and $K = 0, \ldots, M-1$, for some $i_0 \in \mathbb{N}$ and $\eta \in \mathbb{N}$. Note that the argument K in $R_{\eta,l}(K)$ maps to frequency f_K according to

$$f_K = \begin{cases} \frac{K+1-M/2}{MT}, & \text{if } M \text{ is even,} \\ \frac{K-(M-1)/2}{MT}, & \text{if } M \text{ is odd.} \end{cases}$$

Subsequently, the initial Doppler estimate is set to $f_{\bar{K}}$, where

$$\bar{K} = \underset{K}{\operatorname{argmax}} \sum_{\eta=1}^{N} |R_{\eta,l}(K)|^2 ,$$

and N is the number of FFT windows used for acquisition.

4. SIMULATION AND EXPERIMENTAL RESULTS

Simulation results are presented demonstrating the achievable performance of the proposed framework by varying the number of available LEO satellites and the period over which positioning is performed. Experimental results with Orbcomm signals are also presented. The setup used for simulation and experiments is described next. In the following, all position and velocity coordinates are taken in a East-North-Up frame centered at the true receiver position, which is assumed to be stationary.

4.1. Simulation Results

The receiver was located in Riverside, California, U.S.A., and its position estimate was initialized around 28 km away from ground-truth. The simulated LEO satellite trajectories were generated using TLEs of 3 satellite constellations (Orbcomm, Iridium, and Globalstar) with uncertainties of 10 m cross-track and 100 m along-track, emulating somewhat precise knowledge of the orbits. The number of simulated LEO satellites L was varied between 5 and 25 in increments of 5. Note that some satellite trajectories were shifted in time in order to reach the desired number of available satellites. For each value of L, the EKF ran for $\Delta T = 1$, 2, and 4 minutes. The clock drifts were simulated as uniformly distributed random numbers between -50 and 50 m/s. The simulation SNR was chosen to be $\mathrm{SNR}_0 \times \sin el$, where el is the satellite elevation angle, SNR_0 is the SNR at zenith, which was set to 10 dBs, and σ^2_{alt} was set to 1 m^2. The elevation angle mask was set to 10°. The clock drift estimates in the EKF were initialized using the position prior and the first Doppler frequency measurements. The initial estimation error covariance was set to $\mathbf{P}(0|0) \equiv \mathrm{blkdiag}\left[\mathrm{diag}\left[10^8, 10^8, 1\right], 10^3 \mathbf{I}_{L\times L}\right]$. For each $(L, \Delta T)$ pair, 100 Monte Carlo runs were performed. The final position root mean-squared errors (RMSEs) are given in Table 1.

4.2. Experimental Results

An experiment was conducted to demonstrate the proposed navigation framework. To this end, a multipurpose low-cost very high frequency (VHF) dipole antenna and an RTL-SDR dongle were used to sample Orbcomm signals. The samples were stored on a laptop and then processed by the proposed receiver, which was implemented as a software-defined radio (SDR). The true altitude of the antenna was used in the initial position estimate since no altimeter measurements were available. Over the course of the experiment, 2 Orbcomm LEO satellites were available for 60 seconds, one transmitting at 137.3125 MHz and the other at 137.25 MHz. The satellite positions and velocities were obtained using SGP 4 propagation software written in MATLAB and TLE files available online [28]. The EKF was initialized similarly to the simulation results section. The SNR was calculated using the signal-to-variation (SVR) method [29]. The final $xy-$ position error in the EKF was 358 m. The expected Doppler obtained from SGP 4 propagation is shown in Fig. 2(a) along with the Doppler frequencies measured by the proposed SDR. The true receiver position, the final position estimate, and the final position uncertainty ellipse are shown in Fig. 2(b).

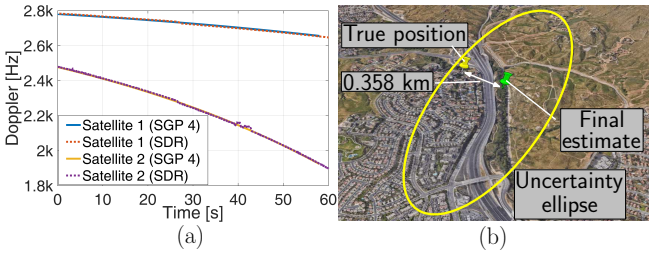

Fig. 2. Experimental results showing (a) the expected and measured Doppler and (b) positioning of a stationary receiver with Doppler measurements from 2 Orbcomm LEO satellites.

4.3. Discussion

It is important to note that in the experiments, the satellite positions and velocities were obtained from the TLE files, which can be off by a few kilometers and meters per seconds, respectively. This is one major source of error that should be considered. One way to account for this source of error is by inflating the measurement noise variance. Furthermore, it was assumed that the receiver and satellite clock drifts were constant, which is not necessarily the case. Moreover, ionospheric and tropospheric delay rates were neglected, which also degrades the positioning performance. Despite these sources of error, the receiver was able to position itself within 360 m from its true position in 1 minute. In the simulation results, an uncertainty of 10 m in the cross-track and 100 m in the along-track were introduced, emulating a more accurate knowledge of the satellite trajectory than in the experiments. Moreover, no model mismatches were introduced (i.e., constant clock drifts and no ionospheric or tropospheric delay rates). Under such conditions, 11 m RMSE can be achieved.

5. CONCLUSION

A framework for positioning with LEO satellite signals was proposed. The framework employs an EKF to estimate a LEO satellite receiver's position using Doppler measurements. The satellites' positions and velocities are known through TLE files. A receiver architecture to extract Doppler measurements from LEO satellite signals was discussed. Simulation results were presented showing that a position RMSE of 11.4 m can be achieved with 25 LEO satellites over a period of 4 minutes. Experimental results were presented demonstrating the proposed receiver positioning itself with 360 m accuracy with real signals from 2 Orbcomm LEO satellites.

6. REFERENCES

[1] G. Seco-Granados, J.A. Lopez-Salcedo, D. Jimenez-Banos, and G. Lopez-Risueno, "Challenges in indoor global navigation satellite systems: unveiling its core features in signal processing," *IEEE Signal Processing Magazine*, vol. 29, no. 2, pp. 108–131, March 2012.

[2] Y. Zhang, M. Amin, and B. Wang, "Mitigation of sparsely sampled nonstationary jammers for multi-antenna GNSS receivers," in *Proceedings of IEEE International Conference on Acoustics, Speech and Signal Processing (ICASSP)*, March 2016, pp. 6565–6569.

[3] E. Axell, E. Larsson, and D. Persson, "GNSS spoofing detection using multiple mobile COTS receivers," in *Proceedings of IEEE ICASSP*, April 2015, pp. 3192–3196.

[4] J. Raquet and R. Martin, "Non-GNSS radio frequency navigation," in *Proceedings of IEEE ICASSP*, March 2008, pp. 5308–5311.

[5] Z. Kassas, "Collaborative opportunistic navigation," *IEEE Aerospace and Electronic Systems Magazine*, vol. 28, no. 6, pp. 38–41, 2013.

[6] J. McEllroy, "Navigation using signals of opportunity in the AM transmission band," M.S. thesis, Air Force Institute of Technology, Wright-Patterson Air Force Base, Ohio, USA, 2006.

[7] S. Fang, J. Chen, H. Huang, and T. Lin, "Is FM a RF-based positioning solution in a metropolitan-scale environment? A probabilistic approach with radio measurements analysis," *IEEE Transactions on Broadcasting*, vol. 55, no. 3, pp. 577–588, September 2009.

[8] M. Joerger, L. Gratton, B. Pervan, and C.E. Cohen, "Analysis of Iridium-augmented GPS for floating carrier phase positioning," *NAVIGATION, Journal of the Institute of Navigation*, vol. 57, no. 2, pp. 137–160, 2010.

[9] T. Reid, A. Neish, T. Walter, and P. Enge, "Leveraging commercial broadband LEO constellations for navigating," in *Proceedings of ION GNSS Conference*, September 2016, pp. 2300–2314.

[10] J. Morales, J. Khalife, A. Abdallah, C. Ardito, and Z. Kassas, "Inertial navigation system aiding with Orbcomm LEO satellite Doppler measurements," in *Proceedings of ION GNSS Conference*, September 2018, pp. 2718–2725.

[11] J. Morales, J. Khalife, C. Ardito, and Z. Kassas, "Simultaneous tracking of Orbcomm LEO satellites and inertial navigation system aiding using Doppler measurements," in *Proceedings of IEEE Vehicular Technology Conference*, 2019, accepted.

[12] C. Ardito, J. Morales, J. Khalife, Ali Abdallah, and Z. Kassas, "Navigation with proposed Starlink satellite signals using Doppler and pseudorange measurements," in *Proceedings of ION International Technical Meeting Conference*, January 2019, accepted.

[13] R. Faragher and R. Harle, "Towards an efficient, intelligent, opportunistic smartphone indoor positioning system," *NAVIGATION, Journal of the Institute of Navigation*, vol. 62, no. 1, pp. 55–72, 2015.

[14] J. Khalife, Z. Kassas, and S. Saab, "Indoor localization based on floor plans and power maps: Non-line of sight to virtual line of sight," in *Proceedings of ION GNSS Conference*, September 2015, pp. 2291–2300.

[15] W. Xu, M. Huang, C. Zhu, and A. Dammann, "Maximum likelihood TOA and OTDOA estimation with first arriving path detection for 3GPP LTE system," *Transactions on Emerging Telecommunications Technologies*, vol. 27, no. 3, pp. 339–356, 2016.

[16] A. Tahat, G. Kaddoum, S. Yousefi, S. Valaee, and F. Gagnon, "A look at the recent wireless positioning techniques with a focus on algorithms for moving receivers," *IEEE Access*, vol. 4, pp. 6652–6680, 2016.

[17] K. Shamaei, J. Khalife, and Z. Kassas, "Exploiting LTE signals for navigation: Theory to implementation," *IEEE Transactions on Wireless Communications*, vol. 17, no. 4, pp. 2173–2189, April 2018.

[18] J. Khalife and Z. Kassas, "Navigation with cellular CDMA signals – part II: Performance analysis and experimental results," *IEEE Transactions on Signal Processing*, vol. 66, no. 8, pp. 2204–2218, April 2018.

[19] Z. Kassas, J. Khalife, K. Shamaei, and J. Morales, "I hear, therefore I know where I am: Compensating for GNSS limitations with cellular signals," *IEEE Signal Processing Magazine*, pp. 111–124, September 2017.

[20] T. Reid, A. Neish, T. Walter, and P. Enge, "Broadband LEO constellations for navigation," *NAVIGATION, Journal of the Institute of Navigation*, vol. 65, no. 2, pp. 205–220, 2018.

[21] D. Lawrence, H. Cobb, G. Gutt, M. OConnor, T. Reid, T. Walter, and D. Whelan, "Navigation from LEO: Current capability and future promise," *GPS World Magazine*, vol. 28, no. 7, pp. 42–48, July 2017.

[22] M. Rice, C. Dick, and F. Harris, "Maximum likelihood carrier phase synchronization in FPGA-based software defined radios," in *Proceeding of IEEE ICASSP*, May 2001, vol. 2, pp. 889–892.

[23] Y. Yang, J. Lie, and A. Quintero, "Low complexity implementation of carrier and symbol timing synchronization for a fully digital downhole telemetry system," in *Proceedings of IEEE ICASSP*, April 2018, pp. 1150–1153.

[24] N. Levanon, "Quick position determination using 1 or 2 LEO satellites," *IEEE Transactions on Aerospace and Electronic Systems*, vol. 34, no. 3, pp. 736–754, July 1998.

[25] N. Nguyen and K. Dogancay, "Algebraic solution for stationary emitter geolocation by a LEO satellite using doppler frequency measurements," in *Porceedings of IEEE ICASSP*, March 2016, pp. 3341–3345.

[26] J. Hamkins and M. Simon, *Autonomous software-defined radio receivers for deep space applications*, chapter 8, pp. 227–270, John Wiley & Sons, Inc, New York, NY, 2006.

[27] A. Oppenheim, W. Ronald, and R. John, *Discrete-time signal processing*, chapter 9, pp. 693–718, Prentice hall, Englewood Cliffs, NJ, 3rd edition, 2009.

[28] D. Vallado and P. Crawford, "SGP4 orbit determination," in *Proceedings of AIAA/AAS Astrodynamics Specialist Conference and Exhibit*, August 2008.

[29] A. Brandao, L. Lopes, and D. McLemon, "In-service monitoring of multipath delay and cochannel interference for indoor mobile communication systems," in *Proceedings of IEEE ICC/SUPERCOMM*, May 1994, vol. 3, pp. 1458–1462.